Turkish Journal of Electrical Engineering & Computer Sciences

http://journals.tubitak.gov.tr/elektrik/

Research Article

Turk J Elec Eng & Comp Sci
(2016) 24: 4582 – 4603

doi:10.3906/elk-1404-250

# A comprehensive control strategy of railway power quality compensator for AC traction power supply systems

**Hamed JAFARI KALEYBAR***, **Siamak FARSHAD**
Department of Railway Engineering, Iran University of Science and Technology, Tehran, Iran

**Received:** 14.04.2014 • **Accepted/Published Online:** 18.08.2015 • **Final Version:** 06.12.2016

**Abstract:** The development of electrical railway systems leads to critical power quality problems in the power grid. This paper discusses a kind of half-bridge-based railway power quality compensator system (HBRPQC) that can compensate negative sequence currents, harmonics, and reactive power simultaneously. In order to keep the HBRPQC performance efficient for the different kinds of transformers used in traction power supply substations, a new multifunctional control strategy that performs better than previous methods is proposed. Due to the fast dynamicity of traction loads, a recessive self-tuning PI controller based on fuzzy logic is adopted in the current control system. The output control variables are integrated with carrier-based pulse width modulation techniques to generate the pulse signals of HBRPQC switches. The performance of the proposed control strategy is verified for V/V, Yd11, and Scott transformers by simulation and the results prove the effectiveness of the strategy.

**Key words:** Half-bridge back-to-back converter, railway power quality compensator, modified-instantaneous p-q theory, fuzzy logic, power quality

## 1. Introduction

Electrical railway systems are considered to be one of the main public transportation systems. These systems have power quality problems that can adversely affect other consumers and equipment at points of common coupling [1–4]. Among these problems, the significant amount of negative sequence current (NSC) that results from single-phase traction loads are worth mentioning. The NSC makes the power network unbalanced [5,6]. Furthermore, traction locomotives have induction motors and are considered as a massive induction load. The overhead catenary system (OCS) also has contact wires that transfer current and power from the traction power supply substations (TPSs) to the train. These wires have an inductive reactance, too. Consequently, the large quantity of reactive power consumed in the traction supply (TS) decreases the power factor of the network [7,8]. Traction loads also consist of power electronic converters functioning as nonlinear loads and producing a wide range of harmonics in the system [9,10]. The abovementioned problems cause undesirable effects in utility power systems, such as vigorous shocks and noises in generators, increases in heat and losses in transformers and transmission lines, bad impacts on protective systems, and failures in the performance of relays [11–14]. In some cases, they can be involved in the instability of power networks, too [15,16]. Over the years, much effort has been put into studies proposing to improve the power quality of TS. To eliminate NSC, special TPS transformers like Scott, impedance-matching, and Woodbridge transformers have been used [17–19]. However, these methods are

*Correspondence: jafarik.hamed@gmail.com

only effective when 2 adjacent sections have equal loads. Moreover, these transformers increase installation costs as well. Various research about flexible alternating current transmission system (FACTS) instruments applied to the TS and long transmission lines for reactive power and NSC compensation has been carried out [20–22], but these compensators are unable to fully compensate for both of the aforementioned parameters. In order to remove harmonics, passive filters and active power filters have been suggested, but they also prove inefficient because they cannot compensate the NSC [23–25]. Thus, a comprehensive compensator in TS was urgently required. The railway power quality compensator system (RPQC) was proposed in Japan [26]. It comprised a couple of back-to-back converters with a common DC-link capacitor. It can compensate harmonics, NSC, and reactive power simultaneously. Much research has been carried out about the configuration and control of RPQC systems. Most of it has chosen a specific TPS transformer for the RPQC configuration. Thus, the introduced control strategies are designed just for the selected transformer [15,27,28]. In other words, in the majority of previous studies, the primary side of TPS transformers is selected as the reference to dissolve equations and extract compensation signals. Because of various connections of transformers in the secondary side, the angles derived from the secondary side are different. Therefore, the compensation equations cannot be generalized for another transformer. Also, in most of the recent studies, the converters of traction locomotives are assumed to be pulse width modulation (PWM) converters and the power factor (PF) is selected as about unity. Consequently, reactive power compensation in these control strategies has not been investigated seriously and completely [15,27,28]. A large number of locomotives still have a thyristor or diode converters in their configuration, which reduces the PF substantially.

In this paper a new control strategy of RPQC systems is proposed that is valid for different kinds of TPS transformers. It is a comprehensive method developed from a modified p-q theory that can compensate NSC, harmonics, and reactive power for loads with nonunity PF.

This paper is organized as follows. Section 2 describes the configuration and operation of the half-bridge-based railway power quality compensator system (HBRPQC) used as a compensator converter. In Section 3 the features and parameters that are important for choosing TPS transformers are evaluated for 3 popular transformers (V/V, Yd11, Scott) and compensation principles for these transformers are analyzed. In Section 4, the compensation control strategy, including reference signal extraction method, recursive PI controller with fuzzy set-point weighting (FSW), and control of DC-link voltage, is studied in detail. In Section 5, simulation results and analysis are presented for the 3 aforementioned transformers. To evaluate the PI FSW controller performance, the results are compared with hysteresis current control (HCC) and the conventional PI method. Finally, Section 6 concludes this paper.

## 2. Traction power supply system with HBRPQC topology

After the appearance of the RPQC, several studies about the topology of this system were published in the literature [29,30]. Most of them evaluated the type of converters and TPS transformers used in the RPQC. They followed some objectives like reliability, decrease in the cost of implementation, and complexity of the control scheme. Recently, a new topology of RPQC that consists of 2 half-bridge converters called the HBRPQC was introduced [31]. Figure 1 represents the configuration of the HBRPQC. As can be seen in this figure, unlike the conventional RPQC, the HBRPQC comprises 2 power switch legs and 2 DC-link capacitors in series. Therefore, because of its features, including lower cost, less complexity, and high reliability, a HBRPQC configuration is chosen in this paper in order to solve the power quality problems of the proposed traction system. The HBRPQC should carry out the compensation duty for all traction network load conditions continuously. It is

assumed that there are 2 traction loads on both sides of the TPS. The load currents of right and left sections are considered as $i_{LR}$ and $i_{LL}$, respectively. These currents are forwarded to the locomotives through the OCS and a pantograph to supply the power needs of the traction motors. To compensate for NSC, harmonics, and reactive power, the currents of the secondary side $(i_R, i_L)$ should be completely sinusoidal, symmetrical, and in the same phase as their voltages $(V_R, V_L)$. To achieve the above purposes, the compensation currents $(i_{rR}, i_{rL})$ are injected into the system through interface inductances $(L_I)$ and step-down transformers with the turn ratio of $K_S$. These compensation signals are produced by a proposed extraction strategy that transfers the active power from the lightly loaded section to the heavily -loaded section and injects extracted reactive and harmonic currents to both sections through the converters.

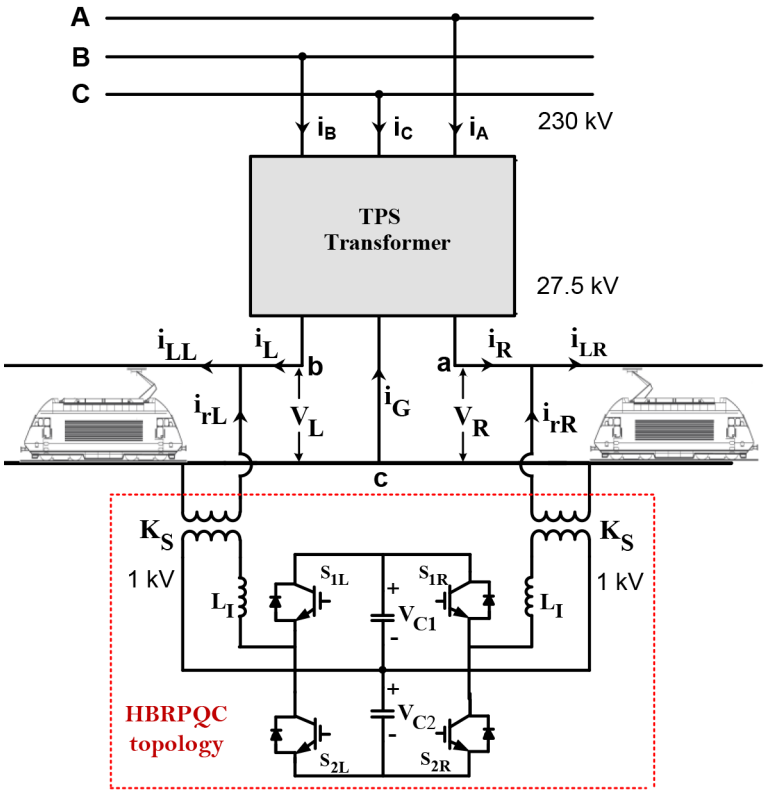


**Figure 1.** TPS configuration with HBRPQC.

## 3. Compensation principles for TPS transformers

### 3.1. TPS transformer's characteristics

Different types of TPS transformers (i.e. V/V, Yd, Scott) are used in electrical railway systems to solve power quality problems. The main task of these transformers is to convert a symmetrical 3-phase voltage to a single-phase voltage supplying the traction load. Figure 2 shows the structure of these transformers. They are selected based on cost and electrical performance. While there are several parameters to assess different structures of transformers, they are evaluated and compared according to these 3 most important factors: transformer utilization factor (TUF), line utilization factor (LUF), and the current unbalance ratio $(\varepsilon)$. These parameters are defined as follows:

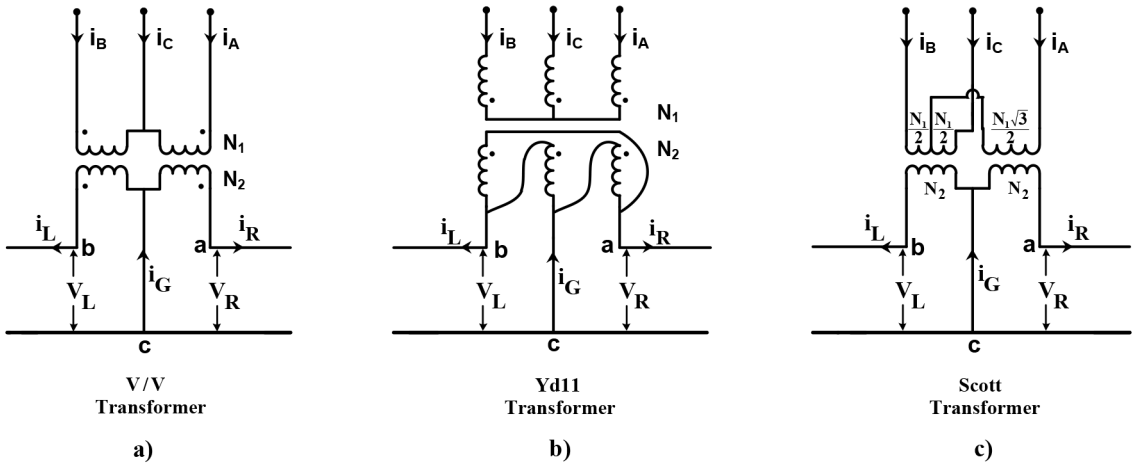


**Figure 2.** Different types of TPS transformers.

$$TUF = \frac{S_R}{S_T} \tag{1}$$

$$LUF = \frac{S_R}{S_L} \tag{2}$$

$$\varepsilon = \frac{|I^-|}{|I^+|} \tag{3}$$

Here, $S_R$, $S_T$, and $S_L$ are maximum capacity utilization, transformer capacity, and line capacity, respectively. $I^-$ is the negative sequence current and $I^+$ denotes the positive sequence current. These 3 factors are affiliated to the load balance ratio expressed as:

$$\zeta = \frac{|I_{light-load\,section}|}{|I_{heavy-load\,section}|} \tag{4}$$

It is important to define and calculate the previous parameters of TPS transformers, which are useful and popular in RPQC systems. All the aforementioned factors were defined for different types of TPS transformers in [32,33]. The calculated results of these parameters, based on the load balance ratio, are summarized in Table 1. As shown in the table, Yd and V/V transformers have lower TUF and LUF, respectively. With respect to the current unbalanced ratio, the Scott transformer has the best performance in comparison to the others. This means that the rate of NSC injected into the 3-phase system is lower in the Scott transformer. However, the Scott transformer, which is known as a balanced transformer, has a complicated and expensive structure. In order to investigate compensation principles, it is necessary to calculate TPS voltages and currents for these transformers.

### 3.2. V/V transformer

The primary side phase voltages are considered as:

$$\begin{cases} \dot{V_A} = Ve^{i0} \\ \dot{V_B} = Ve^{i\frac{4\pi}{3}} \\ \dot{V_C} = Ve^{i\frac{2\pi}{3}} \end{cases} \tag{5}$$

**Table 1.** TPS transformers parameters.

| Parameters | TPS transformer | | |
|---|---|---|---|
| | V/V | Yd | Scott |
| TUF | $\frac{1+\zeta}{2}$ | $\frac{1+\zeta}{2.64}$ | $\frac{3(1+\zeta)}{3+2\sqrt{3}}$ |
| LUF | $\frac{1+\zeta}{3}$ | $\frac{1+\zeta}{2.64}$ | $\frac{1+\zeta}{2}$ |
| $\varepsilon$ | $\frac{\sqrt{\zeta^2-\zeta+1}}{2}$ | $\frac{\sqrt{\zeta^2-\zeta+1}}{2}$ | $\frac{\zeta-1}{\zeta+1}$ |

Therefore, line-to-line voltages on the secondary side are:

$$\begin{cases} \dot{V}_R = \dot{V}_{ac} = \frac{\dot{V}_{AC}}{a} = \frac{\sqrt{3}}{a} V e^{-i\frac{\pi}{6}} \\ \dot{V}_L = \dot{V}_{bc} = \frac{\dot{V}_{BC}}{a} = \frac{\sqrt{3}}{a} V e^{-i\frac{\pi}{2}} \end{cases} \tag{6}$$

Here, $V$ is the effective value of the phase voltage and $a$ is the conversion ratio of the transformer. Considering PF as close to 1, the currents in each section can be calculated as:

$$\begin{cases} i_R = \dot{I}_{ac} = I e^{-i\frac{\pi}{6}} \\ i_L = \dot{I}_{bc} = \zeta I e^{-i\frac{\pi}{2}} \\ i_G = -(\dot{I}_{ac} + \dot{I}_{bc}) = -(I e^{-i\frac{\pi}{6}} + \zeta I e^{-i\frac{\pi}{2}}) \end{cases} \tag{7}$$

$I$ denotes the effective value of current in the secondary side.

According to transformer features, the 3-phase currents of the primary side are:

$$\begin{cases} i_A = \frac{i_R}{a} = \frac{I e^{-i\frac{\pi}{6}}}{a} \\ i_B = \frac{i_L}{a} = \frac{\zeta I e^{-i\frac{\pi}{2}}}{a} \\ i_C = -(i_A + i_B) = -(\frac{I e^{-i\frac{\pi}{6}}}{a} + \frac{\zeta I e^{-i\frac{\pi}{2}}}{a}) \end{cases} \tag{8}$$

The phase diagram of voltages and currents without compensation is illustrated in Figure 3a. As seen in this figure, the current amplitudes of the 2 sections are unbalanced as $\Delta i 4$. Therefore, the 3-phase currents of the primary side are unbalanced in amplitude. As can be seen, due to the V/V connection, these currents are asymmetrical, too. The phase A current lags the phase A voltage by $30^\circ$ and phase B current leads the phase B voltage by $30^\circ$.

### 3.3. Yd transformer

The primary side phase voltages are considered as in Eq. (5). Therefore, line-to-line voltages on the secondary side are:

$$\begin{cases} \dot{V}_R = \dot{V}_{ac} = \frac{\dot{V}_{AC}}{a} = \frac{\sqrt{3}}{a} V e^{i0} \\ \dot{V}_L = \dot{V}_{bc} = \frac{\dot{V}_{BC}}{a} = \frac{\sqrt{3}}{a} V e^{-i\frac{\pi}{3}} \end{cases} \tag{9}$$

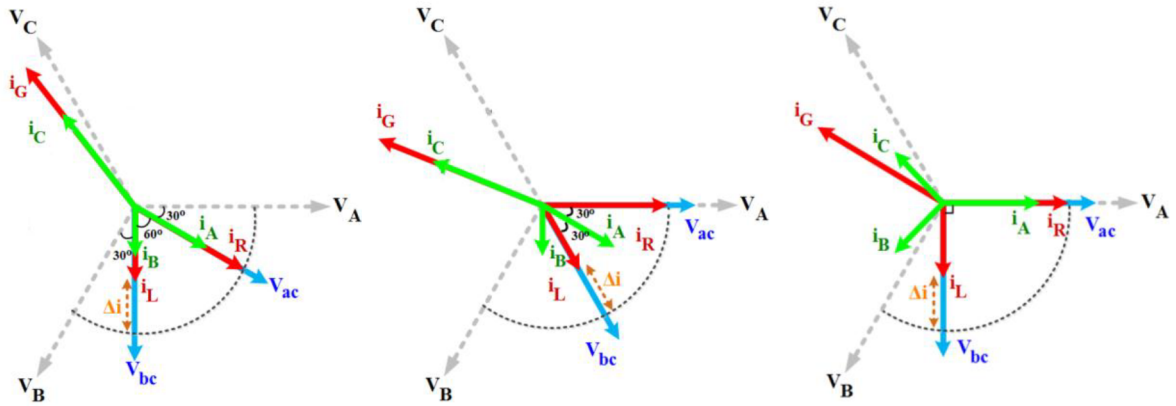


**Figure 3.** TPS phase diagram of voltages and currents before compensation.

Considering a PF close to 1, the current in each section can be calculated as:

$$\begin{cases} i_R = \dot{I}_{ac} = Ie^{i0} \\ i_L = \dot{I}_{bc} = \zeta Ie^{-i\frac{\pi}{3}} \\ i_G = -(\dot{I}_{ac} + \dot{I}_{bc}) = -(Ie^{i0} + \zeta Ie^{-i\frac{\pi}{3}}) \end{cases} \tag{10}$$

According to transformer features, the 3-phase currents of the primary side are:

$$\begin{cases} i_A = \frac{i_R}{a} = \frac{Ie^{i0}}{a} \\ i_B = \frac{i_L}{a} = \frac{\zeta Ie^{-i\frac{\pi}{3}}}{a} \\ i_C = -(i_A + i_B) = -(\frac{Ie^{i0}}{a} + \frac{\zeta Ie^{-i\frac{\pi}{3}}}{a}) \end{cases} \tag{11}$$

The phase diagram of voltages and currents without compensation is illustrated in Figure 3b. As seen in this figure, like the V/V transformer, the current amplitudes of the 2 sections are unbalanced as $\Delta i \text{for} \zeta \neq 1$ and the primary side currents are asymmetrical, too. The phase A current lags the phase A voltage by 30° and phase B current leads the phase B voltage by 30°. The presented equations in this section can be generalized for other Yd transformers vector groups.

### 3.4. Scott transformer

Considering the primary side phase voltages as in Eq. (5), line-to-line voltages on the secondary side are:

$$\begin{cases} \dot{V}_R = \dot{V}_{ac} = \frac{\dot{V}_{AC}}{a} = \frac{\sqrt{3}}{a} Ve^{i0} \\ \dot{V}_L = \dot{V}_{bc} = \frac{\dot{V}_{BC}}{a} = \frac{\sqrt{3}}{a} Ve^{-i\frac{\pi}{2}} \end{cases} \tag{12}$$

Considering the PF as close to 1, the current in each section can be calculated as:

$$\begin{cases} i_R = \dot{I}_{ac} = Ie^{i0} \\ i_L = \dot{I}_{bc} = \zeta Ie^{-i\frac{\pi}{2}} \\ i_G = -(\dot{I}_{ac} + \dot{I}_{bc}) = -(Ie^{i0} + \zeta Ie^{-i\frac{\pi}{2}}) \end{cases} \tag{13}$$

According to transformer features, the 3-phase currents of primary side are:

$$\begin{pmatrix} i_A \\ i_B \\ i_C \end{pmatrix} = \frac{1}{a} \begin{pmatrix} \frac{2}{\sqrt{3}} & 0 \\ \frac{-1}{\sqrt{3}} & 1 \\ \frac{-1}{\sqrt{3}} & -1 \end{pmatrix} \begin{pmatrix} i_R \\ i_L \end{pmatrix} = \frac{1}{a} \begin{pmatrix} \frac{2}{\sqrt{3}} I e^{i0} \\ \frac{-1}{\sqrt{3}} I e^{i0} + \zeta I e^{-i\frac{\pi}{2}} \\ \frac{-1}{\sqrt{3}} I e^{i0} - \zeta I e^{-i\frac{\pi}{2}} \end{pmatrix} \tag{14}$$

The phase diagram of voltages and currents without compensation is illustrated in Figure 3c. As seen in this figure, like V/V and Yd transformers the current amplitudes of the 2 sections are unbalanced as $\Delta i$ for $\zeta \neq 1$ and the primary side currents (phase B and C currents) are asymmetrical, too.

### 3.5. Analysis of compensation principles

Considering the phase diagram of voltages and currents without compensation, the secondary side currents are unbalanced in amplitude as:

$$\Delta i = |i_R| - |i_L| = I\,(1 - \zeta) \tag{15}$$

To balance the amplitude of currents, half of the current difference of the 2 sections should be transferred from the heavily loaded section to the lightly loaded section. This brings the currents of each section as follows:

$$\begin{cases} i'_R = i_R - \frac{\Delta i}{2} e^{i\delta} \\ i'_L = i_L + \frac{\Delta i}{2} e^{i\gamma} \end{cases} \tag{16}$$

$\delta$ and $\gamma$ are the phases of secondary currents, which were calculated in the previous section for different transformers. As illustrated in Figures 4a, 4b, and 4c, after transferring this amount of current, the secondary side currents $(i'_R, i'_L)$ and the consequent primary currents $(i'_A, i'_B)$ now have the same amplitude. Due to the balanced structure of the Scott transformer, with the equalization of current amplitudes, the 3-phase primary side currents get symmetrically in phase, too, but the 3-phase primary side currents of the V/V and Yd11 transformers still are not symmetrical. In order to make the 3-phase currents symmetrical, as illustrated in Figures 5a and 5b, the reactive currents $(i_{qr}, i_{ql})$ should be added to each section. These currents can be calculated as:

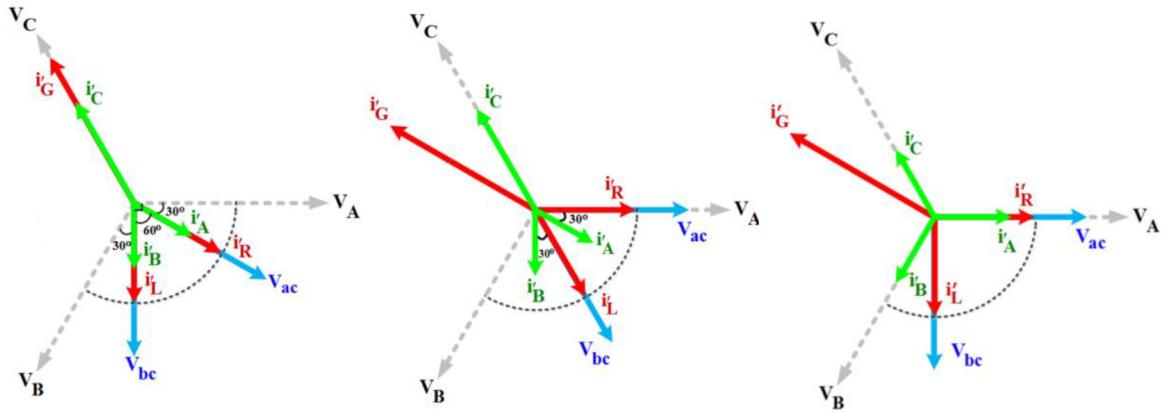


**a) V/V transformer** **b) Yd11 transformer** **c) Scott transformer**

**Figure 4.** TPS phase diagram of voltages and currents after active power transferring.

$$\begin{cases} i_{qr} = tg30^\circ \times \frac{i'_R}{a} e^{i\frac{\pi}{2}} \\ i_{ql} = tg30^\circ \times \frac{i'_L}{a} e^{-i\frac{\pi}{2}} \end{cases} \tag{17}$$

These reactive currents are injected by transferring the reactive power from the lead section to the lag section. Finally, the 3-phase currents of the primary side can be calculated as:

$$\begin{cases} i''_A = i'_A + i_{qr} \\ i''_B = i'_B + i_{ql} \\ i''_C = -(i''_A + i''_B) \end{cases} \tag{18}$$

As shown in Figure 5, these currents are balanced and symmetrical now.

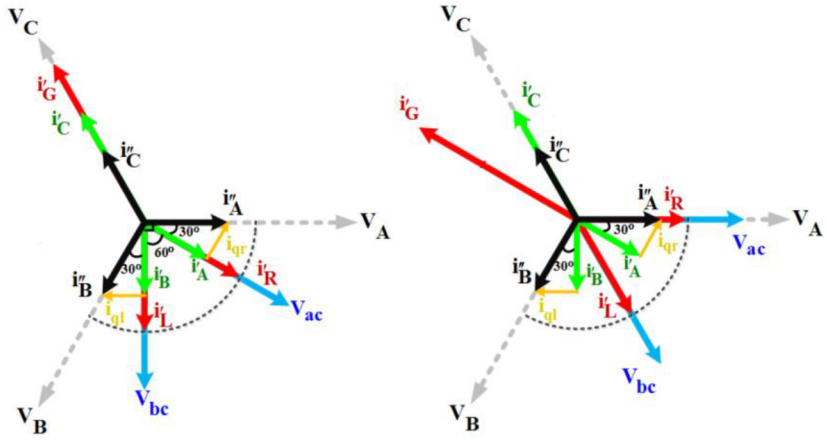


**a) V/V transformer** **b) Yd11 transformer**

**Figure 5.** TPS phase diagram of voltages and currents after active power transferring and reactive power compensation.

## 4. Control of HBRPQC

### 4.1. Extraction strategy of HBRPQC reference signal

In order to calculate compensation currents, voltage and current equations should be written in such a way that the compensation strategy becomes applicable for all kinds of TPS transformers. In most papers, the primary side of TPS transformers is chosen as a set point to extract reference currents, but since the secondary side connections are different, the adopted control scheme is not valid for various TPS transformers. Therefore, in order to design a comprehensive control method, a new strategy based on instantaneous reactive power theory (p-q theory) is proposed. Recently, a hybrid power quality conditioner for a cophase power supply system in an electrified railway using a V/V transformer was proposed in [34,35]. The control strategy of this compensator is based on the single-phase p-q theory, but it was proposed by considering a static traction load in one section and only for a V/V transformer. However, the control strategy proposed in this paper can regulate active and reactive powers in both sections of the TPS instantaneously and dynamically. Furthermore, it can be used for all kinds of TPS transformers. Figure 6 shows the modified control system diagram. As illustrated in this figure, a $\pi/2$ lag of the instantaneous voltages and currents is used to transform the original system into a 2-phase system. Therefore, the obtained system can be represented in an $\alpha\beta$-coordinate system. By using these definitions, the voltages of both sections of the TPS in the $\alpha\beta$-coordinate system are represented as:

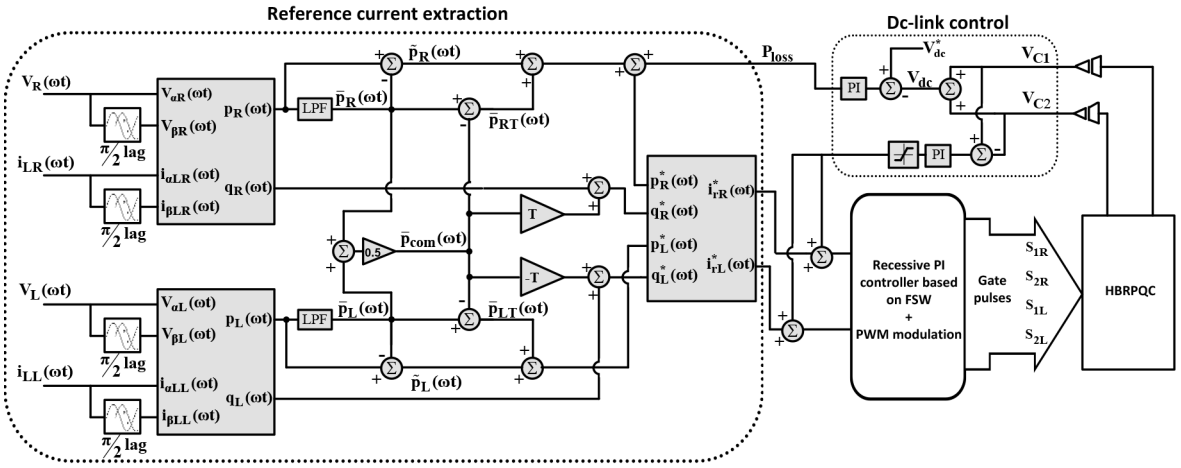


**Figure 6.** Control system of HBRPQC.

$$\begin{pmatrix} V_{\alpha R}(\omega t) \\ V_{\beta R}(\omega t) \end{pmatrix} = \begin{pmatrix} V_R(\omega t) \\ V_R(\omega t) - \frac{\pi}{2} \end{pmatrix} \tag{19}$$

$$\begin{pmatrix} V_{\alpha L}(\omega t) \\ V_{\beta L}(\omega t) \end{pmatrix} = \begin{pmatrix} V_L(\omega t) \\ V_L(\omega t) - \frac{\pi}{2} \end{pmatrix} \tag{20}$$

$V_R(\omega t)$is the instantaneous voltage of the right section and $V_L(\omega t)$ is the instantaneous voltage of the left section. Similarly, the load currents in an $\alpha\beta$-coordinate system are represented as:

$$\begin{pmatrix} i_{\alpha LR}(\omega t) \\ i_{\beta LR}(\omega t) \end{pmatrix} = \begin{pmatrix} i_{LR}(\omega t) \\ i_{LR}(\omega t) - \frac{\pi}{2} \end{pmatrix} \tag{21}$$

$$\begin{pmatrix} i_{\alpha LL}(\omega t) \\ i_{\beta LL}(\omega t) \end{pmatrix} = \begin{pmatrix} i_{LL}(\omega t) \\ i_{LL}(\omega t) - \frac{\pi}{2} \end{pmatrix} \tag{22}$$

Here, $i_{LR}(\omega t)$and $i_{LL}(\omega t)$are instantaneous load currents of the right section and the left section, respectively. The instantaneous active and reactive powers of both sections, as defined in the original 3-phase p-q theory, can be calculated as:

$$\begin{pmatrix} p_R(\omega t) \\ q_R(\omega t) \end{pmatrix} = \begin{pmatrix} V_{\alpha R}(\omega t).i_{\alpha LR}(\omega t) \\ V_{\beta R}(\omega t).i_{\alpha LR}(\omega t) \end{pmatrix} + \begin{pmatrix} V_{\beta R}(\omega t).i_{\beta LR}(\omega t) \\ -V_{\alpha R}(\omega t).i_{\beta LR}(\omega t) \end{pmatrix} \tag{23}$$

$$\begin{pmatrix} p_L(\omega t) \\ q_L(\omega t) \end{pmatrix} = \begin{pmatrix} V_{\alpha L}(\omega t).i_{\alpha LL}(\omega t) \\ V_{\beta L}(\omega t).i_{\alpha LL}(\omega t) \end{pmatrix} + \begin{pmatrix} V_{\beta L}(\omega t).i_{\beta LL}(\omega t) \\ -V_{\alpha L}(\omega t).i_{\beta LL}(\omega t) \end{pmatrix} \tag{24}$$

$p(\omega t)$ and $q(\omega t)$in each section are defined as:

$$\begin{cases} p_R(\omega t) = \bar{p}_R(\omega t) + \tilde{p}_R(\omega t) \\ p_L(\omega t) = \bar{p}_L(\omega t) + \tilde{p}_L(\omega t) \end{cases} \tag{25}$$

$$\begin{cases} q_R(\omega t) = \bar{q}_R(\omega t) + \tilde{q}_R(\omega t) \\ q_L(\omega t) = \bar{q}_L(\omega t) + \tilde{q}_L(\omega t) \end{cases} \tag{26}$$

These 4 powers have constant values and oscillating components. $\bar{p}(\omega t)$ and $\tilde{p}(\omega t)$represent the average and oscillating parts of active power, whereas $\bar{q}(\omega t)$and $\tilde{q}(\omega t)$denote the average and oscillating parts of reactive power. Due to the dynamicity of traction systems, a Bessel-based low-pass filter is used for separating the DC and oscillating parts of power. The DC components are responsible for instantaneous fundamental active and reactive power. Thus, in order to eliminate NSC the required DC active powers in each section can be expressed as:

$$\begin{cases} \bar{p}_{RT}(\omega t) = \bar{p}_R(\omega t) - \bar{p}_{com}(\omega t) \\ \bar{p}_{LT}(\omega t) = \bar{p}_L(\omega t) - \bar{p}_{com}(\omega t) \end{cases} \tag{27}$$

Here, the common constant active power ($\bar{p}_{com}(\omega t)$) is:

$$\bar{p}_{com}(\omega t) = \frac{\bar{p}_R(\omega t) + \bar{p}_L(\omega t)}{2} \tag{28}$$

In other words, some active powers are transferred from the lightly loaded section to the heavily loaded section to make the active currents of the 2 sections balanced in amplitude. To balance the phase currents, it is important to add some reactive power in each section. Therefore, the required powers for compensation can be calculated as in Eq. (29):

$$\begin{pmatrix} p_R^*(\omega t) \\ q_R^*(\omega t) \\ p_L^*(\omega t) \\ q_L^*(\omega t) \end{pmatrix} = \begin{pmatrix} \bar{p}_{RT}(\omega t) + \tilde{p}_R(\omega t) + p_{loss} \\ q_R(\omega t) + (T \times \bar{p}_{com}(\omega t)) \\ \bar{p}_{LT}(\omega t) + \tilde{p}_L(\omega t) \\ q_L(\omega t) - (T \times \bar{p}_{com}(\omega t)) \end{pmatrix} \tag{29}$$

$T$ is a constant that is multiplied by $\bar{p}_{com}(\omega t)$ to compensate for the part of the reactive power caused by the secondary connection of TPS transformer. The value of $T$ for different transformers based on Eq. (17) can be calculated as:

$$T = \begin{cases} tg30^\circ = \frac{1}{\sqrt{3}} \text{ V/V and Yd transformer} \\ tg0^\circ = 0 \text{ Scott transformer} \end{cases} \tag{30}$$

Finally, the reference compensating currents of both sections can be calculated using the following equations:

$$i_{rR}^* = \frac{1}{V_{\alpha R}^2(\omega t) + V_{\beta R}^2(\omega t)} \begin{pmatrix} V_{\alpha R}(\omega t) & V_{\beta R}(\omega t) \end{pmatrix} \begin{pmatrix} p_R^*(\omega t) \\ q_R^*(\omega t) \end{pmatrix} \tag{31}$$

$$i_{rL}^* = \frac{1}{V_{\alpha L}^2(\omega t) + V_{\beta L}^2(\omega t)} \begin{pmatrix} V_{\alpha L}(\omega t) & V_{\beta L}(\omega t) \end{pmatrix} \begin{pmatrix} p_L^*(\omega t) \\ q_L^*(\omega t) \end{pmatrix} \tag{32}$$

### 4.2. Current control strategy based on fuzzy logic

The quality of current controller can influence the accuracy and dynamics of power converters. Up to now, several PWM techniques have been developed to control the current loop. The carrier-based PWM method is

one of these techniques that has some advantages, like good dynamicity, less switching losses, and less total harmonic distortion (THD) in switching waveforms [36]. As railway systems can be affected by noise, load disturbances, and other conditions that cause variations in the structure of the system, the control system should be optimized to achieve an excellent value of the desired dynamic response. The PI controller has a simple structure and high regulation precision. The simplest use of this controller can just achieve zero steady-state errors, but the dynamic performances may not be satisfactory. Therefore, it is preferred to optimize this controller by tuning its parameters. Many tuning methods have been presented in the literature [37]. Among all the methods available, fuzzy set-point weighting is one of the most important ones [38,39]. This method is based on determining PI parameters using fuzzy rules. The proposed control system is illustrated in Figure 7. As illustrated, a recessive PI controller combined with fuzzy systems is selected to improve the performance of the current controller not only to achieve zero steady-state errors but also to enhance the robustness of the controller to track reference harmonic currents. The fuzzification takes 2 inputs, current error $e(t)$, which has a significant impact on steady-state error, and its derivative $de(t)/dt$, which affects the dynamic performance and tracking of reference currents. They are all scaled by coefficients $k_1$ and $k_2$ over the range [–3,3]. In order to prove the superiority of the FSW method, the simulations are accomplished using hysteresis current control (HCC) and conventional PI methods, too. The scale of inputs is designed based on the desired same switching frequency. It is also proportional to the hysteresis bandwidth in the HCC algorithm. The membership functions of fuzzy input and output variables are demonstrated in Figure 8. Seven triangle functions and linguistic values are considered for each variable. The selected fuzzy inference system is the Mamdani model based on a 'min and max' type and the structure of rules is written as:

$$If \text{ e is A and } \frac{de}{dt} \text{ is B Then } \Delta k_p \text{ is C and } \Delta k_i \text{ is D} \tag{33}$$

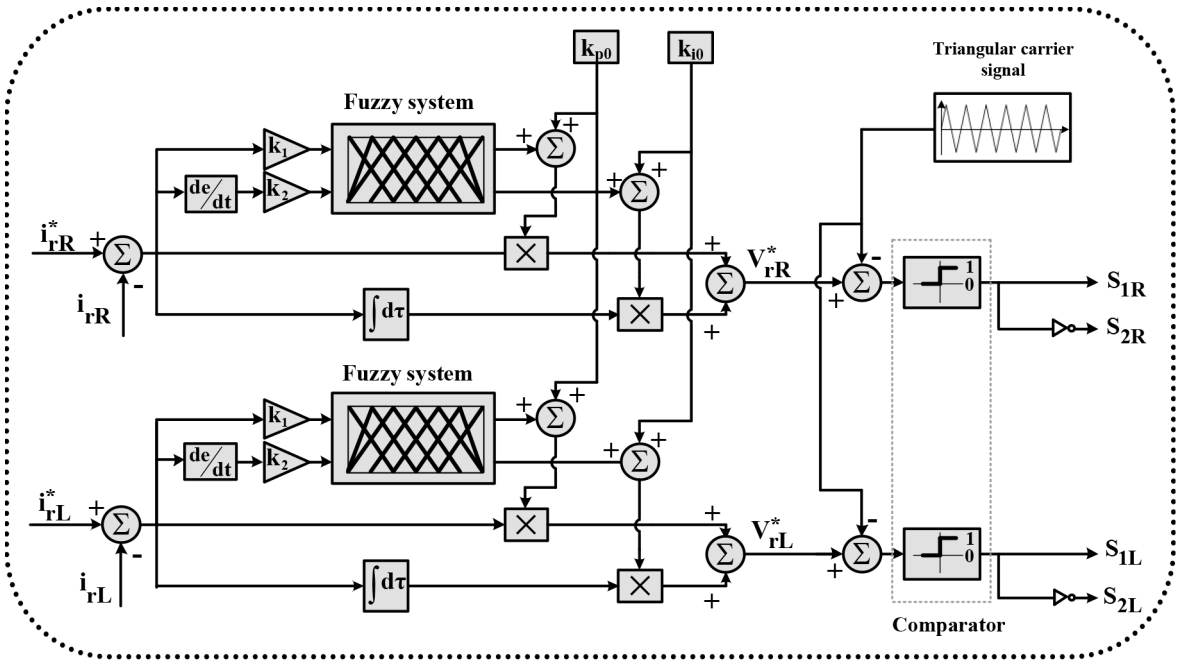


**Figure 7.** Current control system and modulation strategy based on fuzzy logic.

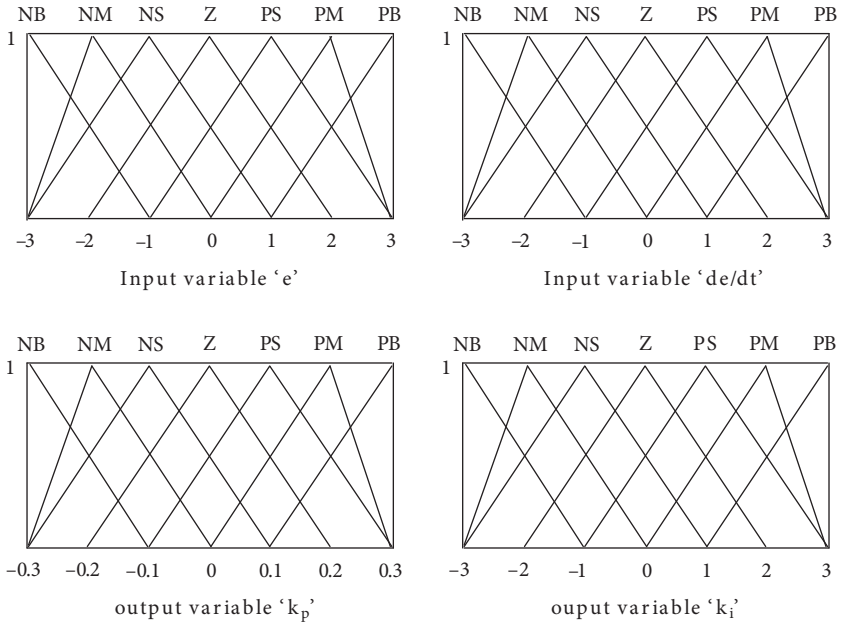


**Figure 8.** Membership functions for inputs and outputs of fuzzy system.

Tables 2 and 3 show the 49 linguistic fuzzy rules for both of the outputs. Here (NB, NM, NS, ZO, PS, PM, PB) is the set of linguistic values, which respectively denote 'negative big', 'negative medium', 'negative small', 'zero', 'positive small', 'positive medium', and 'positive big'. The fuzzy rules surfaces of $\Delta k_p$ and $\Delta k_i$ are demonstrated in Figure 9. The control rules of the fuzzy system are designed carefully to achieve zero steady-state errors and increase the robustness of the control system. In other words, if the output has the desired value ($e(t) = 0$) and the error derivative is zero ($de(t)/dt = 0$) then the output of the controller is kept constant. If the output diverges from the desired value then the necessary action depends on the sign and the value of the error and its derivative. If the conditions are such that the error can be corrected quickly by itself then the controller output is kept constant, or almost constant; otherwise, the controller output will be changed to achieve satisfactory results.

**Table 2.** Fuzzy rules for $k_p$.

| de/dt / e | NB | NM | NS | Z | PS | PM | PB |
|---|---|---|---|---|---|---|---|
| NB | PB | PB | PM | PM | PS | Z | Z |
| NM | PB | PB | PM | PS | PS | Z | NS |
| NS | PM | PM | PM | PS | Z | NS | NS |
| Z | PM | PM | PS | Z | NS | NM | NM |
| PS | PS | PS | Z | NS | NS | NM | NM |
| PM | PS | Z | NS | NM | NM | NM | NB |
| PB | Z | Z | NM | NM | NM | NB | NB |

As can be seen in the current control system, the PI controller form in the time domain is implemented as:

$$u_{PI}(t) = k'_p \cdot e(t) + k'_i \int_0^t e(\tau) \cdot d\tau \tag{34}$$

Here, $u_{PI}(t)$ is the controlling variable, $k'_p$ is adapted proportional gain, and $k'_i$ is adapted integral gain.

**Table 3.** Fuzzy rules for $k_i$.

| e \ de/dt | NB | NM | NS | Z | PS | PM | PB |
|---|---|---|---|---|---|---|---|
| NB | NB | NB | NM | NM | NS | Z | Z |
| NM | NB | NB | NM | NS | NS | Z | Z |
| NS | NB | NM | NS | NS | Z | PS | PS |
| Z | NM | NM | NS | Z | PS | PM | PM |
| PS | NM | NS | Z | PS | PS | PM | PB |
| PM | Z | Z | PS | PS | PM | PB | PB |
| PB | Z | Z | PS | PM | PM | PB | PB |

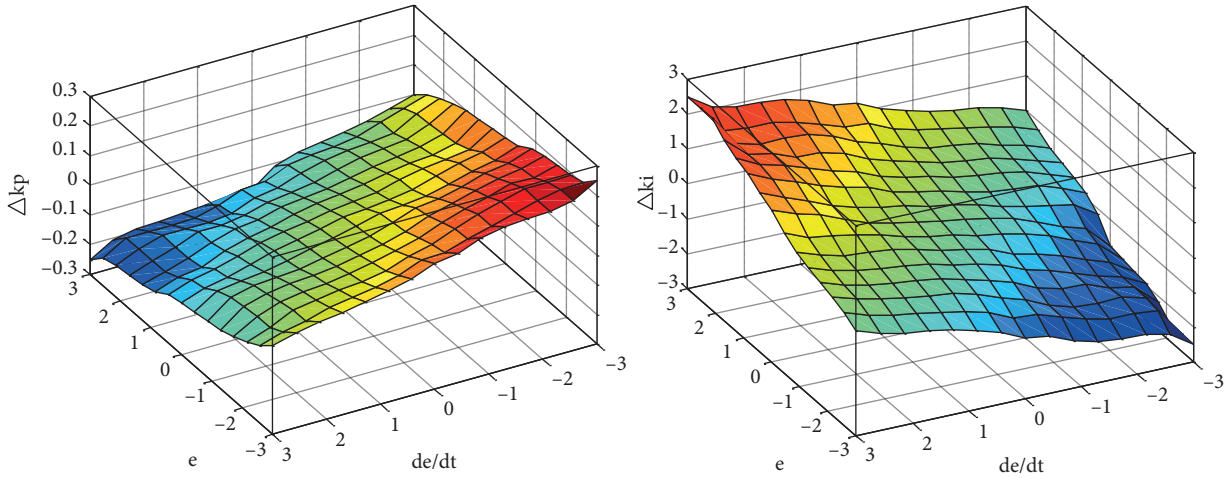


**Figure 9.** Fuzzy rules surface for $k_p$ and $k_i$.

PI self-tuning and adapted correction gains can be made as follows:

$$\begin{cases} k'_p = k_{p0} + \Delta k_p \\ k'_i = k_{i0} + \Delta k_i \end{cases} \tag{35}$$

Here, $k_{p0}$ and $k_{i0}$ are initial value of PI gains, and $k_p$ and $k_i$ are the correctional value of PI gains. The output control variables are compared with a repetitive triangular carrier waveform to generate gate signals of the converter's switch.

### 4.3. Control of DC-link voltage

As described before, the main duty of the HBRPQC is to transfer active and reactive power from one section to the other. In other words, one of the back-to-back converters acts as a rectifier that absorbs the power into the DC-link capacitors and charges them while the other converter acts as an inverter that transfers power to the section with heavy load and therefore discharges the DC-link capacitors. The charging and discharging of DC-link capacitors should be done in such a way that makes the DC-link voltages constant and balanced. Since any fluctuation in this voltage will cause improper performance of the HBRPQC, it should be controlled. To stabilize this voltage, a conventional dual-loop PI controller is used. The PI controller compares the reference

voltage and DC-link voltage to produce the proper control signals. Furthermore, due to the 2 series capacitors, there is a voltage variation problem [40]. If this variation is not controlled, it will lead to unstable system operation. To regulate capacitor voltages, another PI controller is applied to the control loop. First, the voltage variations of capacitors are forwarded to the controller and then the produced output signals are added to the extracted reference currents to eliminate the voltage fluctuation.

The required DC-link capacitances depend on the amount of power transferred by the HBRPQC. The DC-link capacitors can be designed as [41]:

$$\frac{1/2 C_{dc} V_{dc}^2}{P} = (15 - 30)\ ms \tag{36}$$

$P$ is the power rating and $V_{dc}$ is the DC-link voltage, which corresponds to the line voltage as follows:

$$V_{dc} = 1.6 * V_{L-L_{rms}} \tag{37}$$

The amount of charging and discharging time, 15–30 ms, is the empirical value to obtain enough ride-through capability and get 5%–10% voltage ripple [41].

## 5. Simulation results

In order to verify the effectiveness of the proposed compensation and control strategy, simulations based on MATLAB/Simulink software were carried out. Since the low power factor and harmonics are substantial characteristics of railway systems, as illustrated in Figure 10, traction loads are modeled as 2 half-controlled bridge converters connected in series. The simulation parameters of system and traction load are shown in Table 4. Traction load parameters values are transferred to the primary side and the load transformer ratio is 1:0.5:0.5. As explained before, the functionality of the proposed control strategy is independent of TPS transformer type. It is also not affiliated with the vector group of the symmetrical Yd transformer. Therefore, the proposed system is simulated for V/V, Yd11, and Scott transformers separately to prove the validity of the proposed control method. Moreover, to assess the accuracy and dynamic response of the proposed control method, it is assumed that traction loads change on both sides of the TPS. Therefore, simulations are accomplished in 2 steps. First, it is assumed that there is a train in both sections of the TPS and $\zeta = 0.5$. The power of the traction load in feeder 'a' (right section) is 5 MW and in feeder 'c' (left section) is 2.5 MW. The HBRPQC is switched on at t = 0.1 s and compensation is started. The traction load parameters for feeder 'a' are chosen as shown in Table 4. These values are doubled for the load parameters of feeder 'c'. At t = 0.2 s, it is considered that the left section of the TPS has no load ($\zeta = 0$). This process is simulated separately for each current control method and aforementioned transformer. The load currents of the V/V transformer ($i_{LR}$,$i_{LL}$) are illustrated in Figure 11. These currents are similar for the Yd and Scott transformers with phase shifting. As can be seen in this figure, for $\zeta = 0$, since there is no load in the left section, the load current is zero. Figure 12 shows the HBRPQC reference currents ($i_{rR}$,$i_{rL}$) for V/V, Yd11, and Scott transformers. The compensation results of PI FSW, HCC, and conventional PI methods are shown in Figures 13, 14, and 15, respectively. As represented in these figures, before compensation the network-side 3-phase currents are significantly unbalanced and asymmetrical. It can be seen from the simulation results illustrated in Tables 5, 6, and 7 that the unbalanced current ratio ($\varepsilon$) is about 55% and 99% for $\zeta = 0.5$ and $\zeta = 0$, respectively. After turning on the HBRPQC at t = 0.1 s, by transferring power between sections, the network-side 3-phase currents become symmetrical and balanced. Thereupon, as positive and negative sequence currents are shown in the figures, $\varepsilon$ is detracted. In

addition to the NSC, a wide spectrum of harmonics caused by nonlinearity traction loads were also suppressed by the proposed compensation strategies. The THD% of the network-side 3-phase currents, which exceeds 47% in some cases, has been reduced to less than 4%. On the other hand, the considerable amount of reactive power consumed by traction loads makes a low power factor in the power grid. However, as the table shows, after compensation, the power factor has improved from the approximate value of 0.84 to 0.99. It can be seen from the tables that when the compensation system uses the HCC method, the dynamic performance of the compensation system is good, but there is a tracking error in the steady state. The HCC method has a relative superiority in compensation of harmonics, and the THD% of the 3-phase currents in the HCC method is less than in the other methods. When the compensation system uses the PI FSW control method, the steady-state performance is improved compared with the HCC method. In other words, the unbalanced current ratio in PI FSW is less than in the others. However, the conventional PI method has the weakest performance in terms of both accuracy and dynamicity. This can be seen in selected maximized parts of Figures 13–15. Comparing current domains in the figures and the amount of negative sequence current shows that the unbalanced current ratio in the PI method is higher (it exceeds 9% in some cases).

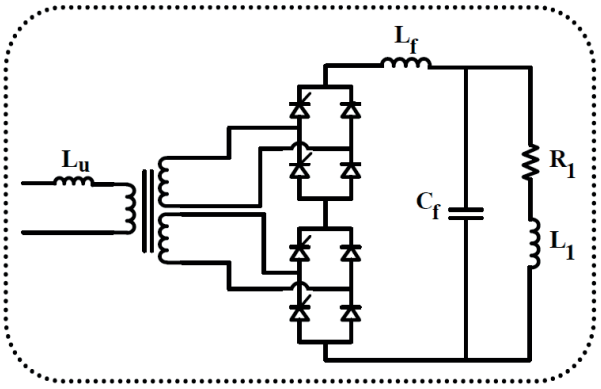


**Figure 10.** Traction load model.

**Table 4.** Parameters of simulation system.

| Parameter | Value |
|---|---|
| TPS transformers ratio ($K_T$) | 230:27.5 |
| Step-down transformers ratio ($K_S$) | 27.5:1 |
| Interface inductance ($L_I$) | 0.5 mH |
| DC-link capacitors ($C_1$, $C_2$) | 40 mF |
| Initial value of proportional gain ($k_{p0}$) | 2 |
| Initial value of integral gain ($k_{i0}$) | 0.1 |
| Proportional gain ($k_p$) | 2 |
| Integral gain ($k_i$) | 0.1 |
| Hysteresis bandwidth (h) | 1 A |
| Traction load inductance ($L_u$) | 9.2 mH |
| Traction load inductance ($L_f$) | 240 mH |
| Traction load capacitor ($C_f$) | 40 $mu$ F |
| Traction load resistor ($R_1$) | 120 Ω |
| Traction load inductance ($L_1$) | 40 mH |

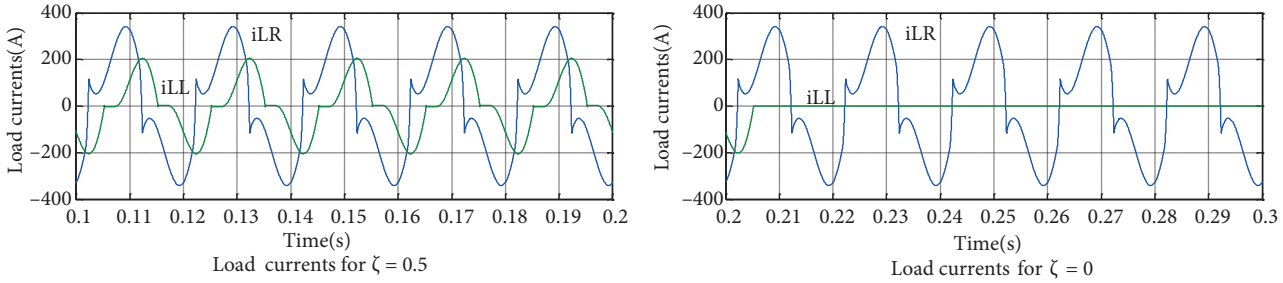


**Figure 11.** Load currents.

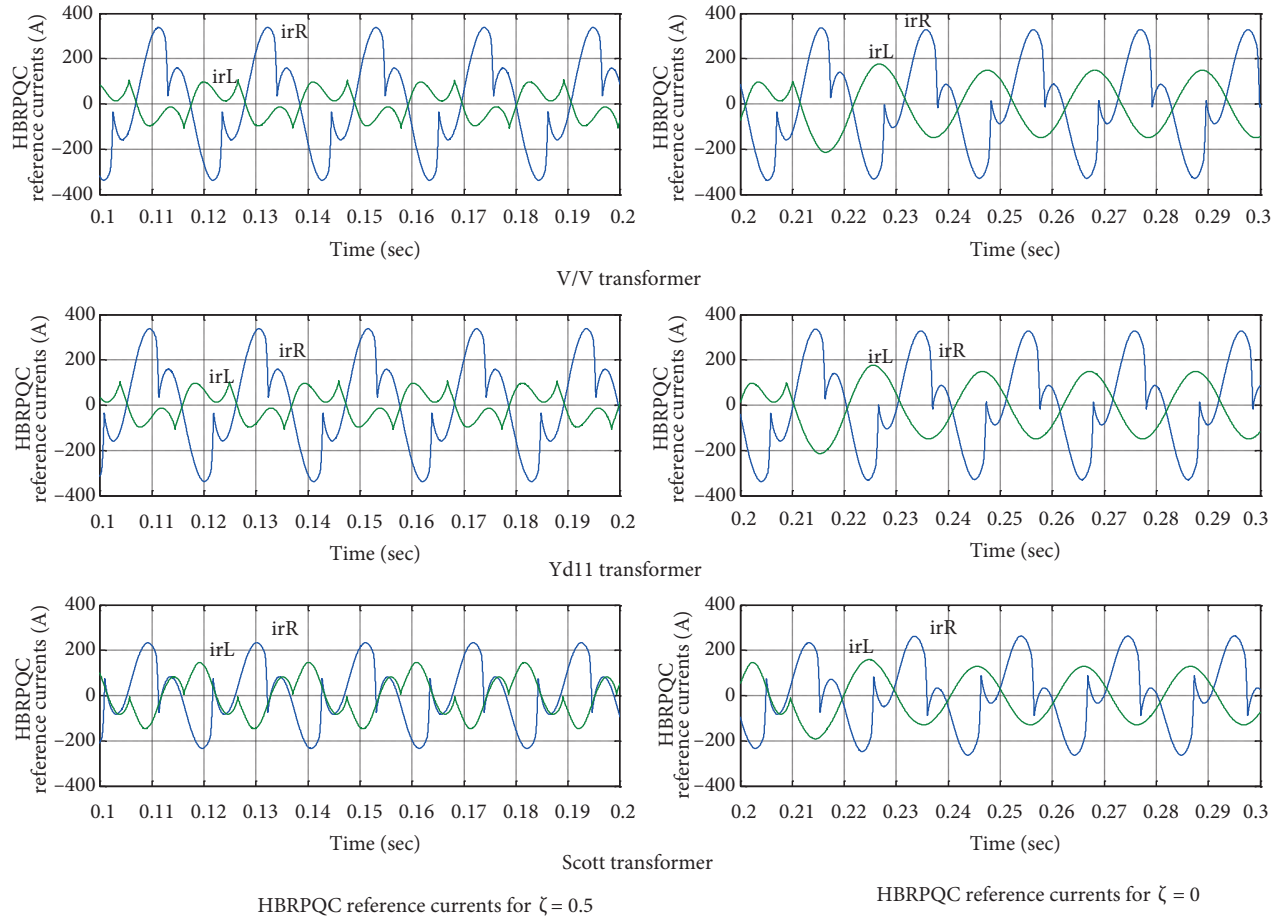


**Figure 12.** HBRPQC reference currents.

The amount of DC-link capacitors designed is based on Eqs. (36) and (37) and considering the worst unbalanced condition ($\zeta = 0$). The amount of power transferred in the formula is considered half of a full traction load (2.5 MW), which leads to 40 mF capacitance. For assessment of the DC-link voltage control strategy, a voltage variation between 2 capacitors is established, so the primary voltages of $C_1$ and $C_2$ are selected as 1200 and 1000 V, respectively. Figure 16 shows the DC-link voltage waveforms. As seen in the figure, after applying HBRPQC at t = 0.1 s, the control strategy regulates capacitor voltages and makes them constant. At t = 0.2 s when the load power level changes, a little voltage fluctuation appears, but it is damped after a regulation time, so the control strategy is fast enough to respond to dynamic changes. The figure also

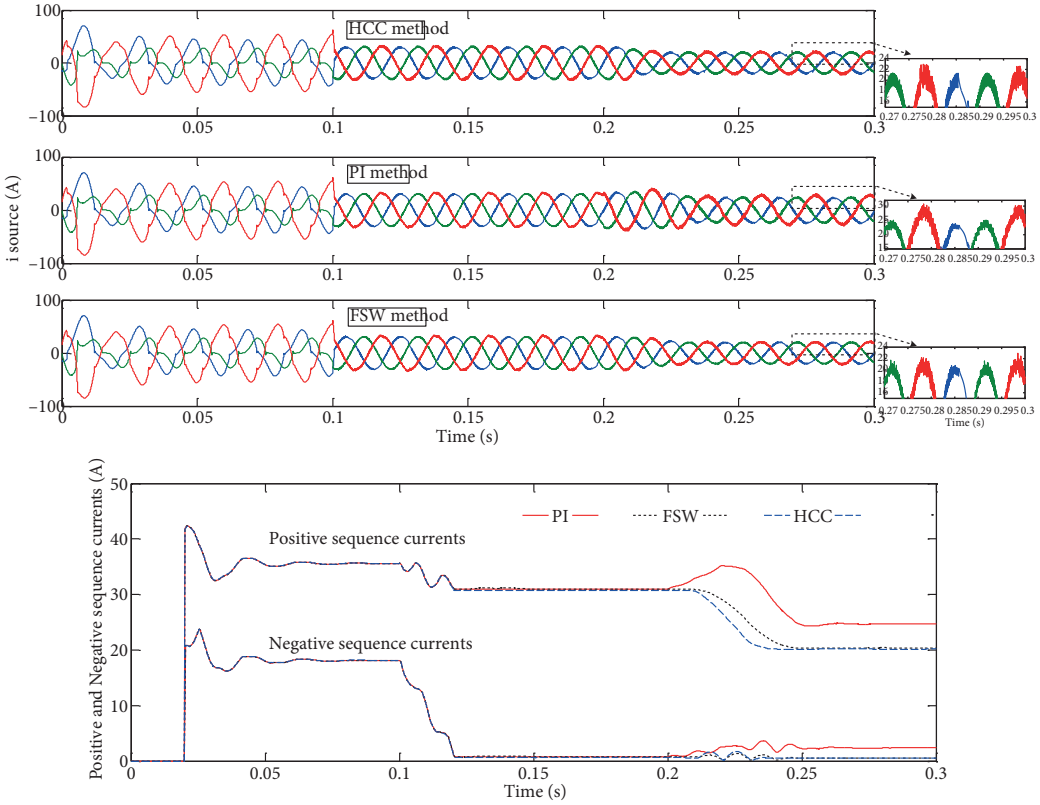


**Figure 13.** Network-side 3-phase currents, positive and negative currents for V/V transformer.

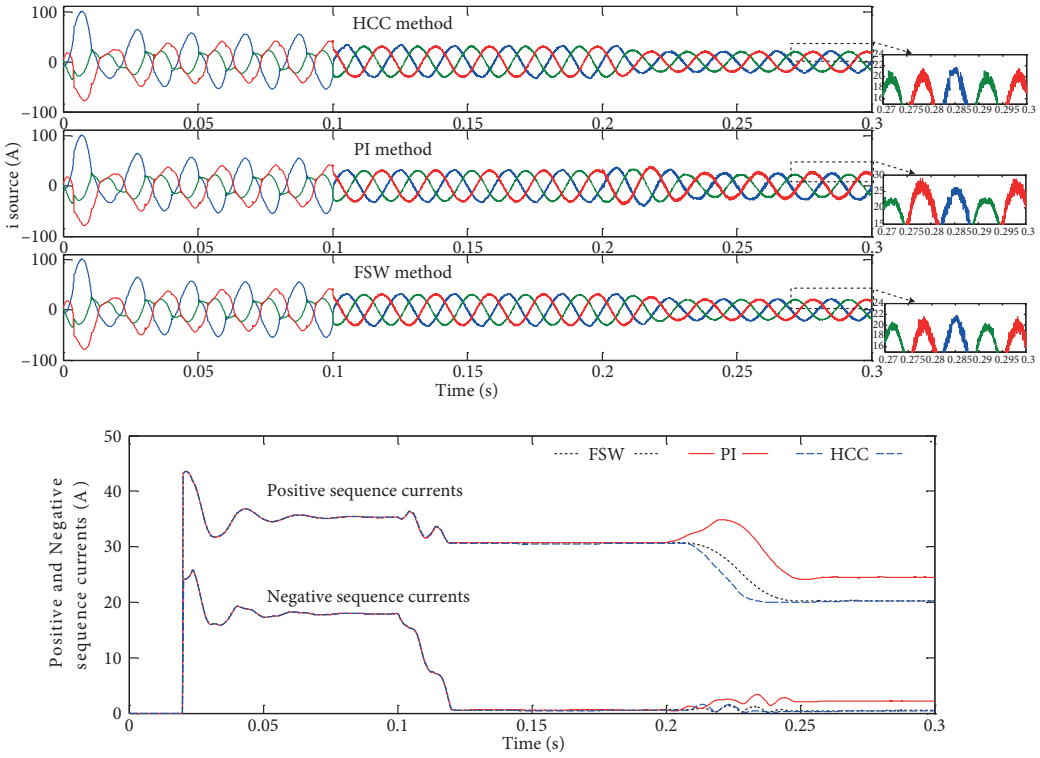


**Figure 14.** Network-side 3-phase currents, positive and negative currents for Yd11 transformer.

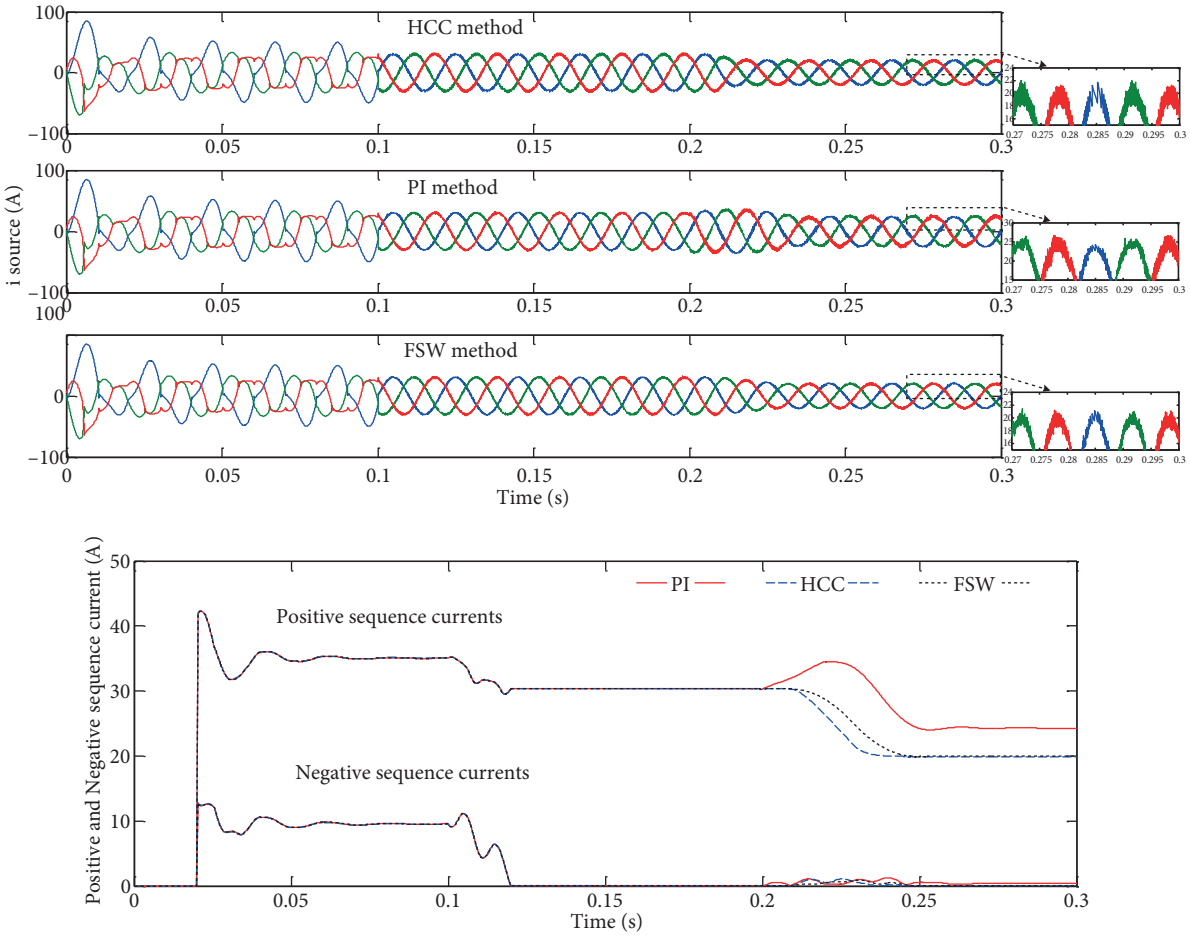


**Figure 15.** Network-side 3-phase currents, positive and negative currents for Scott transformer.

**Table 5.** Simulation results for V/V transformer.

| | | $\zeta = 0.5$ | | | | $\zeta = 0$ | | | |
|---|---|---|---|---|---|---|---|---|---|
| | | Power factor | After compensation | | | Power factor | After compensation | | |
| | | | HCC | PI | FSW | | HCC | PI | FSW |
| THD%of source currents | Phase A | 29.28 | 1.49 | 2.79 | 1.91 | 29.29 | 1.98 | 3.21 | 2.69 |
| | Phase B | 32.37 | 1.05 | 2.74 | 1.04 | 7.85 | 1.22 | 2.11 | 1.55 |
| | Phase C | 16.83 | 1.95 | 2.74 | 2.11 | 29.21 | 2.38 | 3.36 | 2.91 |
| Power factor | | 0.82 | 0.99 | 0.99 | 0.99 | 0.84 | 0.99 | 0.99 | 0.99 |
| $\varepsilon$% | | 54.68 | 2.88 | 3.65 | 1.61 | 97.78 | 3.45 | 9.64 | 2.43 |

**Table 6.** Simulation results for Yd transformer.

| | | $\zeta = 0.5$ | | | | $\zeta = 0$ | | | |
|---|---|---|---|---|---|---|---|---|---|
| | | Power factor | After compensation | | | Power factor | After compensation | | |
| | | | HCC | PI | FSW | | HCC | PI | FSW |
| THD% of source currents | Phase A | 21.78 | 2.21 | 2.50 | 2.30 | 29.47 | 2.85 | 3.16 | 3.11 |
| | Phase B | 47.18 | 1.20 | 1.49 | 1.29 | 29.35 | 0.95 | 2.21 | 1.69 |
| | Phase C | 15.64 | 1.52 | 2.19 | 1.68 | 29.58 | 1.41 | 2.76 | 2.14 |
| Power factor | | 0.84 | 0.99 | 0.99 | 0.99 | 0.85 | 0.99 | 0.99 | 0.99 |
| $\varepsilon$% | | 54.69 | 1.71 | 2.27 | 0.70 | 98.77 | 1.99 | 8.78 | 1.19 |

represents a little variation for capacitor voltages in steady state. It should be noted that these inevitable fluctuations are because of active and reactive power transferring. Therefore, as expected, the DC-link voltages have secondary harmonics that cannot be eliminated.

**Table 7.** Simulation results for Scott transformer.

| | | $\zeta = 0.5$ | | | | $\zeta = 0$ | | | |
|---|---|---|---|---|---|---|---|---|---|
| | | Power factor | After compensation | | | Power factor | After compensation | | |
| | | | HCC | PI | FSW | | HCC | PI | FSW |
| THD% of source currents | Phase A | 21.78 | 1.64 | 2.50 | 2.43 | 29.47 | 2.05 | 3.42 | 3.11 |
| | Phase B | 47.18 | 1.24 | 2.34 | 1.65 | 29.35 | 1.43 | 2.64 | 2.33 |
| | Phase C | 15.64 | 1.30 | 2.23 | 1.57 | 29.58 | 1.25 | 2.53 | 2.32 |
| Power factor | | 0.84 | 0.99 | 0.99 | 0.99 | 0.85 | 0.99 | 0.99 | 0.99 |
| $\varepsilon\%$ | | 54.69 | 0.62 | 0.75 | 0.41 | 98.77 | 0.94 | 1.67 | 0.63 |

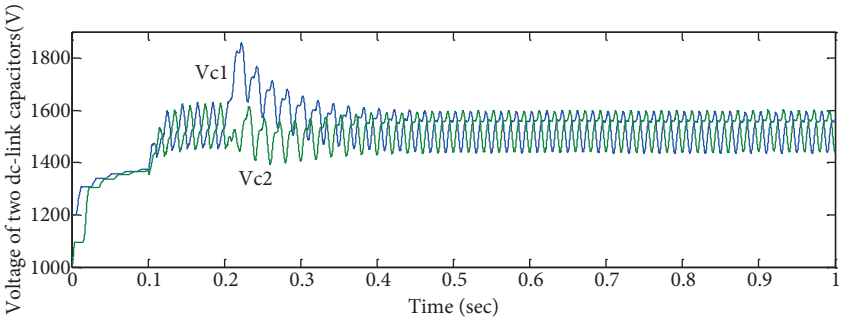


**Figure 16.** Voltage waveforms of 2 DC-link capacitors.

The satisfactory compensation results show that, unlike previous approaches presented in various articles, the proposed control strategy of the HBRPQC works well for different types of TPS transformers.

## 6. Conclusion

In this paper a comprehensive compensation strategy based on a RPQC system is presented for electrical railway power networks to dominate the NSC, suppress harmonics, and compensate reactive power. A new reference current extraction method was introduced in this system, which is applicable to different types of TPS transformers with various connections in the secondary side. Also, unlike the previous methods, the proposed strategy possesses a higher ability to compensate a significant amount of reactive power. In order to have a simple and inexpensive system, the HBRPQC topology is applied to this compensator. Afterwards, to attain a fast and accurate response in the current controller, the carrier-based PWM technique was combined with a recessive PI controller to track reference signals. To achieve zero steady-state errors and increase the robustness of the control system, the FSW method was selected to determine and tune PI parameters. A dual-loop PI controller was used to stabilize voltages of DC-link capacitors and eliminate their fluctuations. Finally, to evaluate the correctness of theoretical analysis of the proposed control method, simulations were carried out for V/V, Yd11, and Scott transformers considering 2 traction load translocations. The simulation results of the PI FSW method were compared with HCC and conventional PI methods. All the results proved the functionality and effectiveness of the proposed strategy.

## References


[1] Sutherland PE, Waclawiak M, Mcgranaghan MF. System impacts evaluation of a single-phase traction load on a 115-kV transmission system. IEEE T Power Deliver 2006; 21: 837-844.

[2] Morrison RE. Power quality issues on ac traction systems. In: IEEE 9th International Conference of Harmonics and Quality of Power; 1–4 October 2000; Orlando, FL, USA. pp. 709-714.

[3] Ozgonenel O, Yalcin T, Guney I, Kurt U. A new classification for power quality events in distribution system. Electr Pow Syst Res 2013; 95: 192-199.

[4] Yalcin T, Ozgonenel O, Kurt U. Feature vector extraction by using empirical mode decomposition for power quality disturbances. In: 10th EEEIC Conference; 8–11 May 2011; Rome, Italy.

[5] Wang H, Tian Y, Gui Q. Evaluation of negative sequence current injection into the public grid from different traction substation in electrical railways. In: IEEE 20th International Conference of Exhibition on Electricity Distribution; 8–11 June 2009; Prague, Czech Republic. pp. 1-4.

[6] Ming-Li D, Guang-Ning W, Xueyuan Z, Chun-Li F, Chang-Hong H, Qiang Y. The simulation analysis of harmonics and negative sequence with a Scott wiring transformer. In: IEEE International Conference of Condition Monitoring and Diagnosis, 21–24 April 2008; Beijing, China. pp. 513-516.

[7] Komrska T, Žák J, Peroutka Z. Reactive power and harmonic currents compensation in traction systems using active power filter with DFT-based current reference generator. In: IEEE 13th European Conference Power Electronics and Applications; 8–10 September 2009; Barcelona, Spain. pp. 1-10.

[8] Coventry A. Resultant reactive power of overhead lines. IEE-Proc C 1956; 103: 334-337.

[9] Lee H, Lee C, Jang G, Kwon S. Harmonic analysis of the Korean high-speed railway using the eight-port representation model. IEEE T Power Deliver 2006; 21: 979-986.

[10] Tan PC, Loh PC, Holmes DG. Optimal impedance termination of 25-kV electrified railway systems for improved power quality. IEEE T Power Deliver 2005; 20: 1703-1710.

[11] Özgönenel O, Terzi ÜK, Khan A. A hybrid approach for power quality monitoring. Turk J Electr Eng Co 2012; 20: 854-869.

[12] Terciyanli A, Açık A, Çetin A, Ermis M, ÇadırcıI, Ermis C, Demirci T, Bilgin HF. Power quality solutions for light rail public transportation systems fed by medium-voltage underground cables. IEEE T Ind App 2012; 487: 1017-1029.

[13] Singh B, Al-Haddad K, Chandra A. A review of active filters for power quality improvement. IEEE T Ind Elec 1999; 46: 960-971.

[14] Ozgonenel O, Thomas DWP, Yalcin T. Superiority of decision tree classifier on complicated cases for power system protection. In: The 11th International Conference on Developments in Power System Protection; 23–26 April 2012; Birmingham, UK.

[15] Wu C, Luo A, Shen J, Ma F, Peng S. A negative sequence compensation method based on a two-phased three-wire converter for a high-speed railway traction power supply system. IEEE T Power Electr 2012; 27: 706-717.

[16] Ozgonenel O, Thomas DWP, Yalcin T, Bertizlioglu IN. Detection of blackouts by using K-means clustering in a power system. In: The 11th International Conference on Developments in Power System Protection; 23–26 April 2012; Birmingham, UK.

[17] Zhang Z, Wu B, Kang J, Luo L. A multi-purpose balanced transformer for railway traction applications. IEEE T Power Deliver 2009; 24: 711-718.

[18] Huang CP, Wu CJ, Chuang YS, Peng SK, Yen JL, Han MH. Loading characteristics analysis of specially connected transformers using various power factor definitions. IEEE T Power Deliver 2006; 21: 1406-1413.

[19] Jafarikaleybar H, Kazemzadeh R, Farshad S. Power rating reduction of railway power quality compensator using Steinmetz theory. In: IEEE International Conference on Power Electronics, Drive Systems & Technology; 3–4 February 2015; Tehran, Iran. pp. 442-447.

[20] Zhu GP, Chen JY, Liu XY. Compensating for the negative sequence currents of electric railway based on SVC. In: Proceedings of the 3rd IEEE Conference on Industrial Electronics Application; 3–5 June 2008; Singapore. pp. 1958-1963.

[21] Sharma PR, Kumar A, Kumar N. Optimal location for shunt connected FACTS devices in a series compensated long transmission line. Turk J Electr Eng Co 2007; 15: 321-328.

[22] Li X, Zuo L. Research on balance compensation of STATCOM. In: Proceedings of the 2nd IEEE Conference on Industrial Electronics Applications; 23–25 May 2007; Harbin, China. pp. 563-568.

[23] Tan PC, Loh PC, Holmes DG. A robust multilevel hybrid compensation system for 25-kV electrified railway applications. IEEE T Power Electr 2004; 19: 1043-1052.

[24] Tan PC, Morrison RE, Holmes DG. Voltage form factor control and reactive power compensation in a 25-kV electrified railway system using a shunt active filter based on voltage detection. IEEE T Ind Appl 2003; 39: 575-581.

[25] Batard C, Machmoum M, Alvarez F, Ladoux P. Control of shunt active power filter for railway sub-station. In: Proceedings of the 32nd IEEE Conference on Industrial Electronics; 6–10 November 2006; Paris, France. pp. 2511-2516.

[26] Mochinaga Y, Hisamizu Y, Takeda M, Miyashita T, Hasuike K. Static power compensator using GTO converters for AC electric railway. In: IEEE Proceedings of the Power Conversation Conference; 19–21 April 1993; Yokohama, Japan. pp. 641-646.

[27] Luo A, Wu C, Shen J, Shuai Z, Ma F. Railway static power compensators for high-speed train traction power supply systems using three-phase V/V transformers. IEEE T Power Electr 2011; 26: 2844-2856.

[28] Shu Z, Xie S, Li Q. Single-phase back-to-back converter for active power balancing, reactive power compensation, and harmonic filtering in traction power system. IEEE T Power Electr 2011; 26: 334-343.

[29] Zhou L, Fu Q, Li X, Liu C. A novel multilevel power quality compensator for electrified railway. In: IEEE Proceedings of the 6th International Conference on Power Electronic Motion Control; 17–20 May 2009; Wuhan, China. pp. 1141-1147.

[30] Sun Z, Jiang X, Zhu D, Zhang G. A novel active power quality compensator topology for electrified railway. IEEE T Power Electr 2004; 19: 1036-1042.

[31] Ma F, Luo A, Xu X, Xiao H, Wu Ch, Wang W. Simplified power conditioner based on half-bridge converter for high-speed railway system. IEEE T Ind Electron 2013; 60: 728-738.

[32] Kalantari M, Sadeghi MJ, Farshad S, Fazel SS. Modeling and comparison of traction transformers based on the utilization factor definitions. International Review on Modelling and Simulations 2011; 4: 342-351.

[33] Kaleybar HJ, Farshad S, Asadi M, Jalilian A. Multifunctional control strategy of half-bridge based railway power quality conditioner for traction system. In: IEEE Proceedings of the 13th International Conference on Environment and Electrical Engineering; 1–3 November 2013; Wroclaw, Poland. pp. 207-212.

[34] Dai NY, Lao KW, Wong MC, Wong CK. Hybrid power quality compensator for co-phase power supply system in electrified railway. IET Power Electron 2012; 5: 1084-1094.

[35] Lao KW, Dai NY, Liu WG, Wong MC. Hybrid power quality compensator with minimum dc operation voltage design for high-speed traction power systems. IEEE T Power Electr 2013; 28: 2024-2036.

[36] Dordevic O, Jones M, Lev E. A comparison of PWM techniques for three-level five-phase voltage source inverters. In: IEEE Proceedings of the 14th International Conference on Power Electronics and Applications; 1 September 2011; Birmingham, UK. pp. 1-10.

[37] Visioli A. Fuzzy logic based set-point weight tuning of PID controllers. IEEE T Syst Man Cy A 1999; 29: 587-592.

[38] Karasakal O, Yeşil E, Güzelkaya M, Eksin İ. Implementation of a new self-tuning fuzzy PID controller on PLC. Turk J Electr Eng Co 2005; 13: 277-286.

[39] Luo A, Ma F, Wu C, Ding SQ, Zhong QC, Shuai Z. A dual-loop control strategy of railway static power regulator under V/V electric traction system. IEEE T Power Electr 2011; 26: 2079-2091.

[40] Uçar M, Özdemir Ş, Özdemir E. A unified series-parallel active filter system for non-periodic disturbances. Turk J Electr Eng Co 2011; 19: 575-596.

[41] Peng FZ, Mckecver JW, Adams DJ. A power line conditioner using cascade multilevel inverters for distribution systems. IEEE T Ind App 1998; 34: 1293-1298.